

## QSO Coronagraphy and Ramp Imaging in the ACS GTO Programs

A. R. Martel<sup>1</sup>, H. C. Ford<sup>1</sup>, G. D. Illingworth<sup>2</sup>, and the ACS Science Team

**Abstract.** We briefly discuss the processing and reduction steps of imaging data acquired in two minor modes of ACS as part of the ACS GTO programs : HRC coronagraphy of the luminous quasar 3C 273 and imaging of nearby early-type galaxies through ramp filters. We show examples of the data at different stages of the analysis. The fully reduced images reveal new morphological features, such as knots and filaments of dust and ionized gas in the ISM of the galaxies, and strong color variations in 3C 273.

### 1. Coronagraphy of the QSO 3C 273

3C 273 was observed with the High Resolution Channel in coronagraphic mode through the *g* (F475W), *V* (F606W), and *I* (F814W) filters on 19/20 Jul 2002 UT. Short target acquisition frames (10 sec through F502N) served to translate the QSO under the central 1".8-diameter occulting spot to an accuracy of 0.5-0.8 pixels. Two orbits were dedicated to each bandpass with a CR-SPLIT of 2 per orbit. The spatial scale at the detector was binned to 0".025 pixel<sup>-1</sup>, resulting in a nominal field-of-view of 25" × 25". A reference star, HD 105281, with colors similar to those of the QSO, was observed in one orbit in the same bandpasses for accurate PSF subtraction.

The PSF of the reference star was used to remove the unresolved QSO. The PSF was manually registered and subtracted via cubic convolution interpolation until the residuals in the wings were visually minimized. The registration appears sensitive to 0.05 pixels and the largest observed shift between the PSF and QSO was 0.8 pixels. The PSF normalization was also manually adjusted until the contribution of the telescope PSF was visually minimized. Past experience indicates that this normalization method is accurate to  $\approx 1\%$ . The images were finally corrected for geometric distortion.

For comparison, the HRC/F606W frame before and after subtraction of the reference PSF is shown in Fig. 1. Before the subtraction (top panel), the most prominent feature is a scattered light bar, symmetric about the PSF. It is found to expand proportionately with wavelength - it might be due to large angle diffraction or a directional wavefront error. Residual diffraction rings are observed around the central spot after the PSF subtraction (bottom panel). These are caused by mismatches between the QSO and reference PSFs, specifically by differences in their positions relative to the center of the occulting spot. A color map produced from the final PSF-subtracted images is shown in Fig. 2. A detailed description of the colors and morphological features in 3C 273 can be found in Martel et al. (2003) and in the STScI press release 2003-3.

---

<sup>1</sup>Department of Physics and Astronomy, Johns Hopkins University, 3400 N. Charles Street, Baltimore, MD 21218

<sup>2</sup>UCO/Lick Observatory, University of California, Santa Cruz, CA 95064

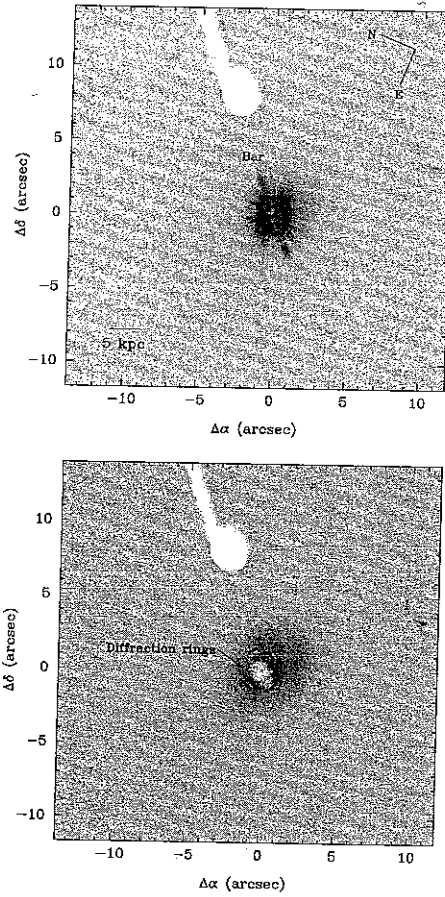


Figure 1: HRC/F606W frame of 3C 273 before (top) and after (bottom) subtraction of the QSO with a reference PSF.

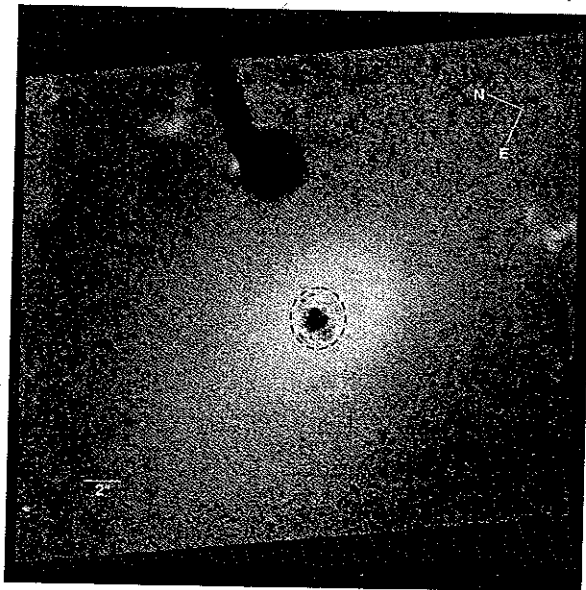


Figure 2:  $gVI$  color map of 3C 273. The dashed circle delimits the residual diffraction rings around the central occulting spot.

## 2. Ramp Imaging of Nearby Ellipticals

Four early-type galaxies were observed for one orbit in the FR656N filter over their redshifted  $H\alpha + [N II]$  emission-line complex and in a broad-band filter, F555W or F814W, adjacent in wavelength, for continuum subtraction. The broad-band exposures were limited to a total duration of 700 sec to avoid overhead penalties in the dumping of the on-board buffer memory and the remainder of the orbit was dedicated to the ramp exposure, typically 1400-1700 sec. The exposures were split into two sub-exposures for a more effective rejection of cosmic ray hits and/or hot pixels. The images were processed with the ACS Science Analysis Pipeline at Johns Hopkins University. The spatial scale of the final, reduced images is  $0''.05 \text{ pixel}^{-1}$ , resulting in a nominal field-of-view of  $3.5 \times 3.5 \text{ arcmin}^2$ .

To extract the pure emission-line maps, the intensity levels between the broad- and ramp images were matched using the counts in a small region in the host galaxy. The scaled continuum image was then subtracted from the ramp image. Ratios calculated with the SYNPHOT *calcpHOT* task in PyRAF with a template spectrum give very similar results. The line fluxes were measured by summing the counts in regions with positive line emission. This usually required delimiting the regions visually with polygons, boxes, and/or ellipses in SAOImage *ds9*. The conversion factor between the observed flux expressed in counts  $\text{sec}^{-1}$  and the physical flux in standard units of  $\text{ergs sec}^{-1} \text{ cm}^{-2}$  was calculated with *calcpHOT*. The fluxes were then corrected for interstellar extinction.

A "dust map" was also generated for each galaxy by calculating the ratio of the continuum image over its isophotal model generated with the PyRAF *ellipse* task. Pixel values less than one represent dusty regions. Two examples, NGC 2832 and NGC 6166, are shown in Fig. 3. Several new, resolved dust and ionized gas features are detected in these galaxies, some on kpc scales. Further details can be found in Martel et al. (2004).

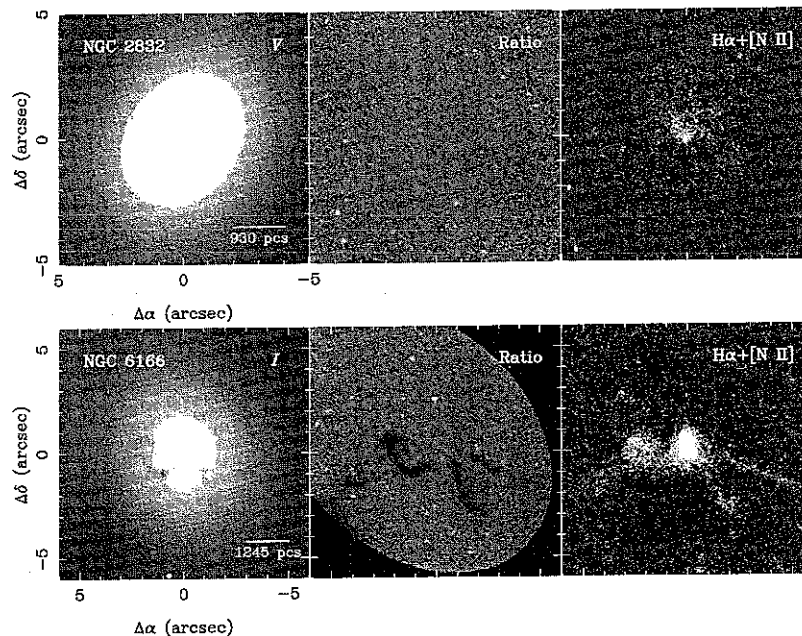


Figure 3: The continuum image, the dust map, and the  $H\alpha + [N II]$  emission-line map (extracted from the FR656N image) of NGC 2832 and NGC 6166 are displayed on a linear scale.

**Acknowledgments.** We are grateful to T. Allen, K. Anderson, and J. McCann for processing and archiving the ACS GTO data presented here.

**References**

- Martel, A.R., Ford, H.C., Tran, H.D., Illingworth, G.D., Krist, J.E., White, R.L., Sparks, W.B., Gronwall, C., Cross, N.J.G., Hartig, G.F., Clampin, M., Ardila, D.R., Bartko, F., Benítez, N., Blakeslee, J.P., Bouwens, R.J., Broadhurst, T.J., Brown, R.A., Burrows, C.J., Cheng, E.S., Feldman, P.D., Franx, M., Golimowski, D.A., Infante, L., Kimble, R.A., Lesser, M.P., McCann, W.J., Menanteau, F., Meurer, G.R., Miley, G.K., Postman, M., Rosati, P., Sirianni, M., Tsvetanov, Z.I., & Zheng, W. 2003, *AJ*, 125, 2964
- Martel, A.R., Ford, H.C., Bradley, L.D., Tran, H.D., Menanteau, F., Tsvetanov, Z.I., Illingworth, G.D., Hartig, G.F., & Clampin, M. 2004, *AJ*, 128, 2758